# Colloidal heat engine driven by engineered active noise

John A. C. Albay,[1,2] Zhi-Yi Zhou,[1] Chia-Hao Chang,[3] Hsuan-Yi Chen,[1,4,5] Jae Sung Lee,[6] Cheng-Hung Chang,[3,5] and Yonggun Jun[1,4,*]

[1]*Department of Physics, National Central University, Taoyuan City 320, Taiwan*
[2]*Department of Mathematics and Physics, College of Science, University of Santo Tomas, Manila 1008, Philippines*
[3]*Institute of Physics, National Yang Ming Chiao Tung University, Hsinchu, 300, Taiwan*
[4]*Center for Complex Systems, National Central University, Taoyuan City 320, Taiwan*
[5]*Physics Division, National Center for Theoretical Sciences, Taipei 10617, Taiwan*
[6]*School of Physics, Korea Institute for Advanced Study, Seoul 02455, Korea*

(Received 13 January 2023; accepted 7 September 2023; published 25 September 2023)

A recent experiment demonstrated that a colloidal heat engine immersed in an active bath can outperform those subject to equilibrium or passive baths. Although it has motivated several theoretical studies to clarify the possible origins of such high efficiency, the discussed noise effects are often intertwined and hard to distinguish in nature. In this paper, we used the optical feedback trap to mimic a colloidal heat engine in various active baths in a precisely controllable setting to analyze the impacts of individual noise properties in real systems. Our experiment, together with theoretical calculations, show that the efficiency of the active engine can be greatly increased when the magnitude of the active-bath noise with a nonzero correlation time is modulated according to the variation of the confining potential in the quasistatic limit. This result reveals how to tune the noise properties of an active bath to enhance the efficiency of a microscopic machine, which could be used to manipulate the functions of stochastic systems under complex active backgrounds.

DOI: 10.1103/PhysRevResearch.5.033208

## I. INTRODUCTION

The study of heat engines is a cornerstone of classical thermodynamics, and their efficiencies are upper bounded by thermodynamic principles [1]. Over the last two decades, advances in miniaturization technology have enabled us to manipulate microscopic systems with significant thermal fluctuations. One prominent example is the demonstration of microscopic heat engines made of a colloidal particle confined by a cyclically varying harmonic potential and subject to a thermal bath [2–6]. As molecules constituting that equilibrium bath are not self-propelled, the engines immersed in it are called a "passive" (bath heat) engine [PBHE, Fig. 1(a)]. The maximum efficiency of a PBHE occurs in the quasistatic cycle, which is further bounded by the Carnot limit.

Recently, more attention has been paid to "active baths," the nonequilibrium reservoirs consisting of active particles. Examples include baths of bacteria [7–9], active nematics [10–12], and Janus particles [13,14]. The noise provided by an active bath is dubbed an "active noise." This noise usually yields unique phenomena different from those of equilibrium baths. For instance, when a tracer particle is immersed in active noise, one would observe enhanced diffusion and specific persistence (correlation) times. An engine subject to an active noise is called an "active" (bath heat) engine [ABHE, Fig. 1(b)]. An example of this engine type is the colloidal Stirling engine in a bacterial bath studied by Krishnamurthy *et al.* [15]. This ABHE was shown to have an efficiency higher than that of its PBHE counterpart. Such high performance is then analyzed and ascribed to the non-Gaussianity and persistent motion of the colloidal particle by the authors. However, several later theoretical studies suggested that non-Gaussianity does not interfere with the energetics of heat engines in the quasistatic limit [16–19], which was also experimentally confirmed recently [20] although it alters the energetic statistics in the finite cycle time. Although there have been a variety of such theoretical analyses on the individual effects of different noise parameters, they are hard to decouple and distinguish in real bacterial experiments. In this paper, we use the optical feedback trap technique to experimentally mimic an active colloidal heat engine, which can be subjected to arbitrary heat baths and confinements. It allows us to systematically survey a broad range of influences of individual noise parameters. Special focus is put on how the stiffness-dependent protocol of the active noise with nonzero correlation times could challenge the upper bound of the engine efficiency. Interestingly, a similar stiffness-dependent temperature has been used to construct a pseudoadiabatic protocol [4], to maintain a constant variance of particle position under quasistatic driving.

## II. ACTIVE ENGINE MODEL

Let us imagine a Brownian particle in water subject to thermal noise $\xi$ and active noise $\zeta$ and confined by a one-dimensional harmonic potential $U(x,t) = (1/2)\kappa(t)x^2$ of

*yonggun@phy.ncu.edu.tw

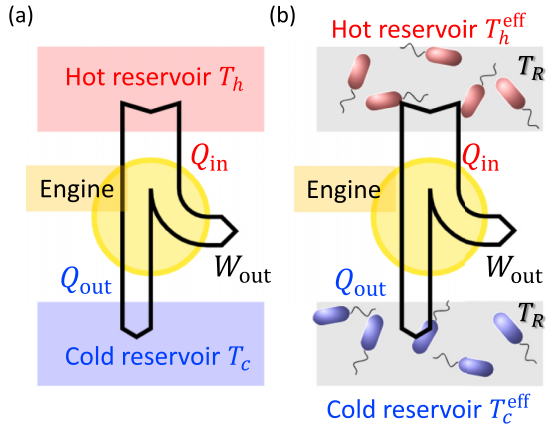


FIG. 1. Schematic example of a microscopic heat engine in contact with (a) an equilibrium and (b) a nonequilibrium heat bath. The blue and red bacteria in (b) represent low and high activity, respectively.

stiffness $\kappa$. The dynamics of the particle position $x$ is described by an overdamped Langevin equation

$$\gamma \frac{dx}{dt} = -\kappa x + \xi + \zeta, \tag{1}$$

where $\gamma$ is the friction coefficient. The thermal force $\xi(t)$ has a zero mean and correlation $\langle \xi(t)\xi(t')\rangle = 2\gamma k_{\rm B} T_{\rm R} \delta(t-t')$, where $T_{\rm R}$ is the real temperature of water (passive bath), $k_{\rm B}$ denotes the Boltzmann constant, $\delta(t-t')$ represents the Dirac delta function, and $\langle\cdot\rangle$ stands for an ensemble average throughout this work. By contrast, the nonequilibrium random noise $\zeta(t)$, despite also having a zero mean, is endowed with the correlation $\langle \zeta(t)\zeta(t')\rangle = \gamma k_{\rm B} T \exp(-|t-t'|/\tau_c)/\tau_c$. Here, $\tau_c$ is the correlation time, and $T$ represents a "nonequilibrium temperature" that a colloidal particle experiences when it diffuses in a potential-free space merely subject to $\zeta$ and in the absence of $\xi$. Notably, $T$ is a kind of noise strength different from the thermodynamic temperature $T_{\rm R}$ [16]. The memory effect of $\zeta(t)$ is characterized by $\tau_c$, which is a factor that makes ABHE perform differently from PBHE [17,18]. This effect is known to capture the key noise statistics of a bacterial bath on a colloidal particle [21,22], and will be generated by the active Ornstein-Uhlenbeck process (AOUP) [23]. Combining $T_{\rm R}$ and $T$, we obtain an effective temperature $T_{\rm eff} \equiv \kappa\langle x^2\rangle/k_{\rm B} = T_{\rm R} + T/(1+\kappa\tau_c/\gamma)$ [16,24] (see Sec. I in the Supplemental Material (SM) [25]). Here, we focus on protocols of $T_{\rm eff}$ instead of other definitions of temperature because $T_{\rm eff}$ is the experimentally more easily measurable and commonly used quantity, which describes the direct effect of active and thermal noises on the colloids in the harmonic potential. Such $T_{\rm eff}$ is a commonly adopted definition of temperature to discuss the thermodynamic energetics of engines, even in the latest Refs. [17,18]. We note that although only the Gaussian AOUP is studied below, our conclusion applies to general non-Gaussian active noises as well, as long as the latter has the same noise correlation function [19,28].

To study the detailed effect of active noise on engine efficiency, we need to control $T$ and $\tau_c$ independently. This is not feasible in a bacterial bath because a way of controlling one parameter usually affects the other. However, such control is not a problem in our correlated noise by using the optical feedback trap (see Secs. II and III in SM [25]). This technique applies an optical force to the colloidal particle from optical tweezers to simultaneously create a "virtual" potential of stiffness $\kappa$ [29,30] and a "virtual" temperature $T$ of the noise [6,31,32]. We first tested the generation of the active noise according to the difference equation (S12) and calibrated it for various $\tau_c$'s (see Sec. III in SM [25]). After this calibration, it is ensured that the potential and noise of a desired ABHE are simultaneously realized. We set the correlation time $\tau_c = 20$ ms during the measurements, which cannot be too large due to the appropriate linear range of the optical force of the optical tweezers being approximately $\pm 150$ nm.

## III. ISO-$T$ HEAT ENGINE

With this setup, we are concerned with a Stirling engine for the colloidal particle. It consists of four processes [Fig. 2(a)]: two iso-$T$ and two iso-$\kappa$ processes. The cycle time $\tau$ ranges from 1 ms to 1 s, and each process lasts for $\tau/4$. The maximum and minimum values of $\kappa$ are $\kappa_h = 20$ pN/μm and $\kappa_l = 10$ pN/μm, respectively. We call this active engine an "iso-$T$ engine." Unlike the iso-$T$ engine with varying $T_{\rm eff}$ during its iso-$T$ process, consider a passive bath Stirling engine [pbSE, red curve in Fig. 2(a)], whose $T$ and $T_{\rm eff}$ are both constant during the iso-$T$ processes. An example is shown in Fig. S4(b), where $T = 200$ and 700 K correspond to $T_{\rm eff} =$ 500 and 1000 K, respectively. Figure 2(b) is the measured variance of the particle position for the iso-$T$ engine at $\tau = 1$ s averaged over 1000 cycles. It agrees well with the theoretical calculation, which justifies that the engine at $\tau = 1$ is in the quasistatic limit.

The engine efficiency is defined as $\eta_z = -\langle W_{\rm out}\rangle/\langle Q_{\rm in}\rangle$, where $z = a$ and $p$ represent ABHE and PBHE, respectively, and $-W_{\rm out}$ and $Q_{\rm in}$ are the work extracted and the heat injected during a single cycle, respectively. The signs of work and heat are positive if energy enters the system. In Fig. 2(c), the $\eta_a$ of the iso-$T$ engine is compared with the $\eta_p$ of the pbSE for various $\tau$. The theoretical calculations of $-W_{\rm out}$ and $Q_{\rm in}$ of iso-$T$ and pbSE are presented in Eqs. (S24) and (S21) of SM [25], respectively. For a cycle time $\tau < 100$ ms, $\eta_a$ is negative so that the engine cannot extract work from the active heat bath. As $\tau$ increases, $\eta_a$ approaches the efficiency at the quasistatic limit, $\eta_{a,\infty} \approx 0.15$ (blue dashed line). However, this $\eta_{a,\infty}$ is still less than the efficiency of quasistatic pbSE $\eta_{p,\infty} \approx 0.29$ (red dashed line).

Figure 2(d) shows the cumulative work $w(t) = \int_0^t (\partial U/\partial\kappa)\dot{\kappa}\,dt'$ for the iso-$T$ engine (blue) and pbSE (red). The $w(t)$ of the latter decreases more rapidly with time than the former. The fluctuations of $W_{\rm out}$ for the iso-$T$ engine are more apparent than those of pbSE [the inset of Fig. 2(d)]. These work fluctuations can be clearly seen from their probability distribution $P(\beta W_{\rm out})$ in Fig. 2(e), with $\beta \equiv (k_{\rm B} T_{\rm R})^{-1}$. The $P(\beta W_{\rm out})$ of the iso-$T$ engine is wider, but has a lower negative mean value compared to that of the pbSE. On the other hand, the difference between the distributions of two $Q_{\rm in}$ is small. The smaller mean value in work, together with the similar distribution in heat, accounts for why the iso-$T$ engine has a lower efficiency.

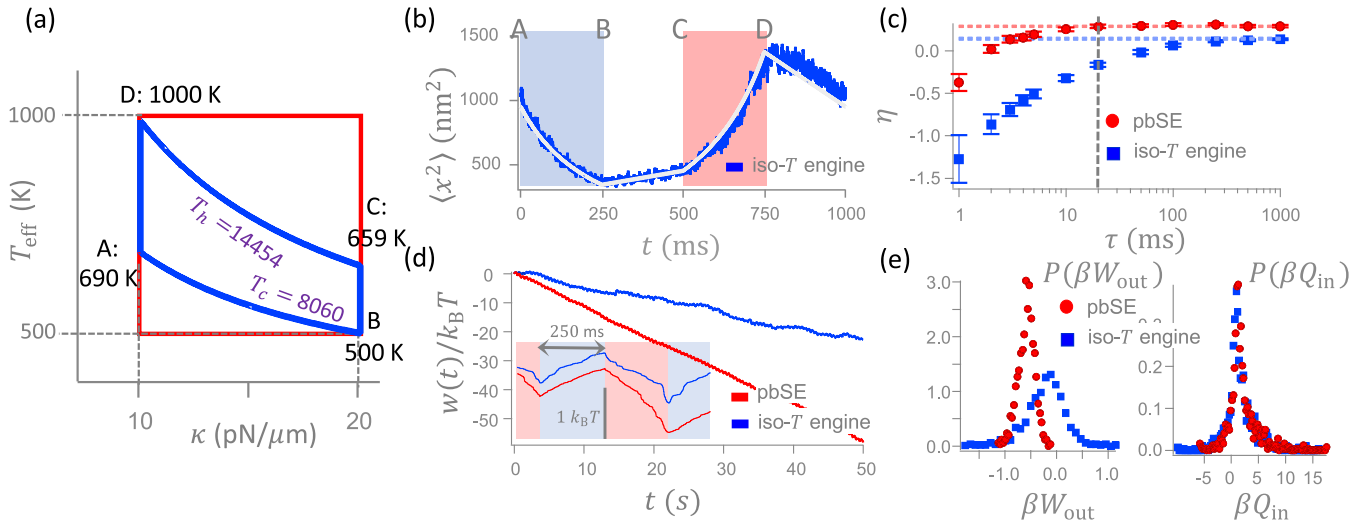


FIG. 2. The energetics of iso-$T$ engine and a pbSE. (a) The theoretical protocol of an iso-$T$ engine (blue) and a pbSE (red). The purple (black) texts refer to the temperature $T$ (effective temperatures $T_{\rm eff}$). (b) The blue curve is the variance of the measured particle position in an iso-$T$ engine. The white curve is the theoretical prediction. (c) The efficiencies of the iso-$T$ engine and the pbSE. The two horizontal dashed lines denote the quasistatic efficiencies for these two engines. Error bars were obtained from bootstrap using 1000 resamplings of size 1000. (d) Cumulative works are extracted from the iso-$T$ and pbSEs for $\tau = 1$ s. Only the works during the processes **AB** and **CD** in each cycle are plotted here. The magnified plot in the inset shows the work trajectory of the two iso-$T$ processes within a cycle. The light blue and red backgrounds represent the iso-$T$ compression and expansion, respectively. The vertical bar denotes the energy scale of work in the inset. (e) Distributions of work (left) and heat (right) for a single cycle.

## IV. ACTIVE BATH HEAT ENGINES WITH ENGINEERED ACTIVE NOISE

As demonstrated above, the efficiency of the iso-$T$ engine is lower than that of pbSE. To enhance the efficiency of the active engine, we modify the temperature protocol $T$, which is constant for the iso-$T$ engine, in such a way that $T$ depends linearly on $\kappa$ during the process **AB** and **CD**. Specifically, let us take $T(\kappa) = T^{\rm A} + a(\kappa - \kappa_l)$ for process **AB**, such that it reaches $T^{\rm B} = T^{\rm A} + a(\kappa_h - \kappa_l)$ at the end of the process, where $a$ is a control parameter to vary the rate of increase of $T$. Similarly, let us select $T(\kappa) = T^{\rm C} + b(\kappa - \kappa_h)$ for the process **CD** with $T^{\rm D} = T^{\rm C} + b(\kappa_l - \kappa_h)$ at the end of the process, where $b$ is another control parameter. Then, the effective temperatures in the process **AB** and **CD** become $T_{\rm eff}(\kappa) \equiv T_{\rm R} + T^{\rm A} f(\kappa)$ and $T_{\rm R} + T^{\rm C} g(\kappa)$, respectively, where $f(\kappa) = [1 + a(\kappa - \kappa_l)/T^{\rm A}]/(1 + \kappa\tau_c/\gamma)$ and $g(\kappa) = [1 + b(\kappa - \kappa_h)/T^{\rm C}]/(1 + \kappa\tau_c/\gamma)$. For comparison, we also studied a PBHE guided by a stiffness-dependent temperature, whose $T_{\rm eff}(\kappa) \equiv T_{\rm R} + [T^{\rm A} + a'(\kappa - \kappa_l)]$ and $T_{\rm R} + [T^{\rm C} + b'(\kappa - \kappa_h)]$ for processes **AB** and **CD**, respectively, with a linear dependence of $T$ on $\kappa$ as above and two other control parameters $a'$ and $b'$. These two parameters are generally different from $a$ and $b$ and are selected to let PBHE have the same $T_{\rm eff}$ as the ABHE at **A**, **B**, **C**, and **D** [see Fig. 3(a)].

Figure 3(a) shows three examples of the above-mentioned stiffness-dependent protocol. First, the green cycle is the protocol of a Stirling-like engine in the $(T_{\rm eff}, \kappa)$ space, where $T_{\rm eff}$ are constant, but its $T$ varies during the process **AB** and **CD**. This is the case when $a = a_{\rm crit}$ and $b = b_{\rm crit}$, where $a_{\rm crit} = T^{\rm A}\tau_c/(\gamma + \kappa_l\tau_c)$ for $T^{\rm A}_{\rm eff} = T^{\rm B}_{\rm eff}$ and $b_{\rm crit} = T^{\rm C}\tau_c/(\gamma + \kappa_h\tau_c)$ for $T^{\rm C}_{\rm eff} = T^{\rm D}_{\rm eff}$. Next, the red cycle follows a protocol with $0 \leqslant a < a_{\rm crit}$ and $0 \leqslant b < b_{\rm crit}$ and the blue cycle follows another protocol with $a > a_{\rm crit}$ and $b > b_{\rm crit}$. The values of $a/a_{\rm crit}$, $b/b_{\rm crit}$, $T^{\rm A}$, $T^{\rm B}$, $T^{\rm C}$, and $T^{\rm D}$ used in the experiment are given in Table I of SM [25]. For all three cycles, the initial and final temperatures and stiffnesses in each process have the same values as those of the cycle in Fig. 2.

Figure 3(b) represents $\langle Q_{\rm in}\rangle_\infty$ and $\langle W_{\rm out}\rangle_\infty$ for various values of $a$, where $\langle\cdot\rangle_\infty$ denotes the ensemble average at the quasistatic limit ($\tau = 1$ s). For comparison, we also realized PBHEs with the same $T_{\rm eff}$ and $\kappa$ at the beginning and end of each process as those of ABHEs. The corresponding $a'$ and $b'$ are also given in Table I of SM [25]. $\langle\beta Q_{\rm in}\rangle_\infty$ (open symbols) and $-\langle\beta W_{\rm out}\rangle_\infty$ (solid symbols) increase with $a$ for $a < a_{\rm crit}$ and decrease with $a$ for $a > a_{\rm crit}$. They both have maximum values at $(a_{\rm crit}, b_{\rm crit})$, where the variation of $T_{\rm eff}$ in ABHE becomes the same as that of PBHE when $(a', b') = (a'_{\rm crit}, b'_{\rm crit}) \equiv (0, 0)$. Compared to $\langle Q_{\rm in}\rangle_\infty$ and $-\langle W_{\rm out}\rangle_\infty$ of the PBHE (circles), those of the ABHE decay slower with $a$ when $a > a_{\rm crit}$.

We compare the efficiency $\eta_a$ of ABHE with the efficiency $\eta_p$ of PBHE as a function of $a/a_{\rm crit}$ in Fig. 3(c). For $a < a_{\rm crit}$, $\eta_a$ (squares) is always lower than $\eta_p$ (circles), consistent with our common impression of less efficient ABHEs. However, the former catches up with the latter at $a = a_{\rm crit}$ and even overtakes the latter at $a > a_{\rm crit}$. The theoretical calculation in Eqs. (S27) and (S30) [solid line in Fig. 3(c)] also predicts the same crossover of efficiency at $a = a_{\rm crit}$. Why ABHE can outperform PBHE at $a > a_{\rm crit}$ is because $W_r$ decreases more slowly than $Q_r$ in Fig. 3(b), where $W_r$ ($Q_r$) denotes the ratio of work (heat) of ABHE to that of the PBHE. We address that such an outperformance is compared between two slightly different cycles [solid and dashed lines in Fig. 3(a)] in the $(\kappa, T_{\rm eff})$ space. To make the PBHE cycle in Fig. 3(a) completely the same as that of ABHE in the same plot, $T$ of

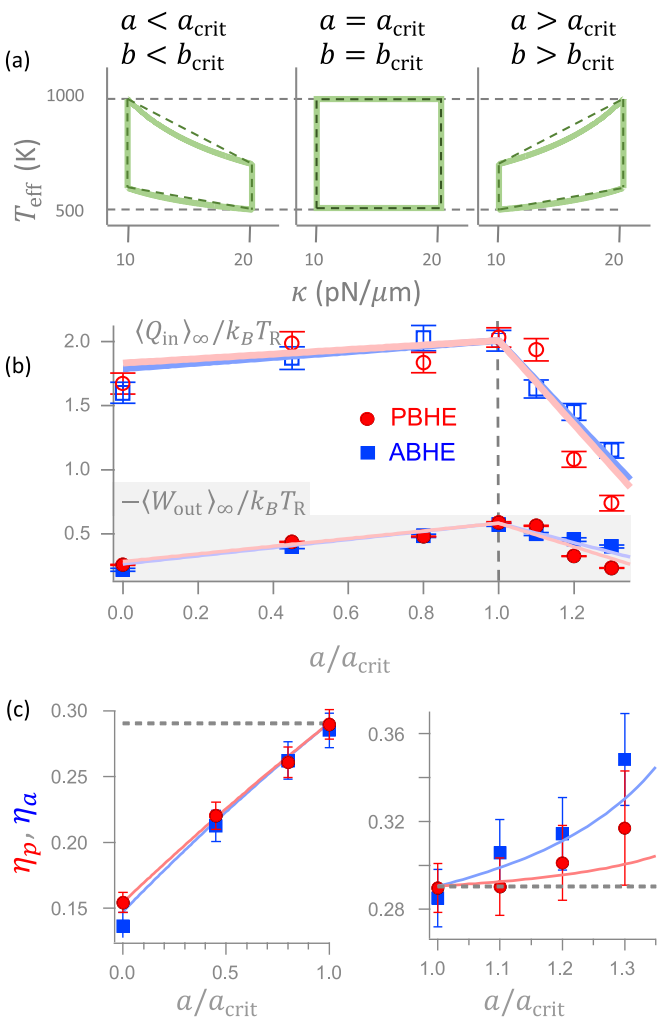


FIG. 3. (a) Three types of the $T_{\rm eff}$-dependent theoretical protocol, $a < a_{\rm crit}$ (left), $a = a_{\rm crit}$ (middle), and $a > a_{\rm crit}$ (right), for the ABHE (solid lines) and their corresponding PBHE (dashed lines). (b) Work $-\langle\beta W_{\rm out}\rangle_\infty$ and heat $\langle\beta Q_{\rm in}\rangle_\infty$ as a function of $a/a_{\rm crit}$. The cycle time is $\tau = 1$ s for all measurements. Error bars were obtained from bootstrap using 1000 resamplings of size 1000. (c) The efficiencies of the ABHE (blue squares) and PBHE (red circles) as a function of $a/a_{\rm crit}$. Error bars were obtained by the same method used in (b). The solid lines are the theoretical curves of Eq. (S27) for the ABHE and of Eq. (S30) for the PBHE. The dashed line is the efficiency of the quasistatically operating pbSE, Eq. (S21).

the former needs to have a sophisticated nonlinear dependence on $\kappa$. Instead of that, we take a specific linear dependence to make the two cycles close to each other. With this simple approach, Fig. 3(c) reveals the essential role of a stiffness-dependent noise strength to obtain a high-efficiency engine. $Q$ is the effective thermal heat exchanged with the bath when $\tau_c = 0$. When $\tau_c$ is nonzero, $Q$ contains extra stochastic work performed by the active components of the bath. The latter is what can be converted directly into extracted work, bypassing the passive limit.

To check whether ABHE can outperform reference PBHE for other $\Delta T_{\rm eff} = T_{\rm eff,h} - T_{\rm eff,c}$ and $\tau_c$, a further experiment was performed, where $T_{\rm eff,h}$ ($T_{\rm eff,c}$) denotes hot (cold) $T_{\rm eff}$ in Fig. 2. It was carried out at fixed $a/a_{\rm crit} = 1.3$ and

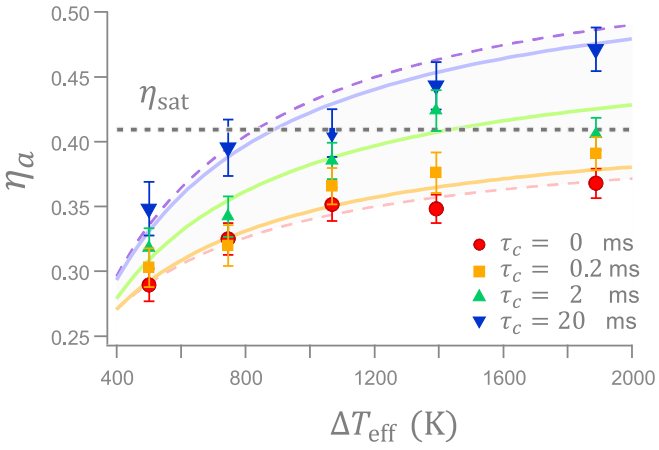


FIG. 4. The efficiencies of the ABHE as a function of $\Delta T_{\rm eff} = T_{\rm eff}^{\rm C} - T_{\rm eff}^{\rm A}$ at $a/a_{\rm crit} = 1.3$ and $b/b_{\rm crit} = 1.6$ for four values of $\tau_c$: 0 (circle), 0.2 (square), 2.0 (up triangle), and 20.0 (down triangle) ms. The three solid (two dashed) lines are the theoretically predicted efficiencies at $\tau_c = 0.2$, 2.0, and 20.0 ms ($\tau_c = 0$ and $\infty$ ms). The lines at $\tau_c = 0$ (pink) and $\infty$ (purple) are the lower and upper bounds of the efficiency, respectively. The horizontal dashed line is the efficiency $\eta_{\rm sat}$ of the pbSE at $\Delta T_{\rm eff} \to \infty$. The four kinds of symbols stand for experimental data. Error bars were obtained from bootstrap using 1000 resamplings of size 1000.

$b/b_{\rm crit} = 1.6$, with the same $\kappa$ as before, but a different range of $\Delta T_{\rm eff}$ from 500 to 1890 K. During the cycles, $T_{\rm eff,h} = T_{\rm eff}^{\rm C}$ was adjusted under a fixed $T_{\rm eff,c} = T_{\rm eff}^{\rm A}$. Figure 4 presents the efficiency of the ABHE as a function of $\Delta T_{\rm eff}$ for four different values of $\tau_c$. Here, the saturated efficiency (horizontal dashed line), $\eta_{\rm sat} = \ln(k_{\rm h}/k_{\rm l})/[1 + \ln(k_{\rm h}/k_{\rm l})] \approx 0.41$, is the maximum efficiency of the pbSE, which is achieved in the limit of $\Delta T_{\rm eff} \to \infty$. The efficiency of ABHE, $\eta_a$, monotonically increases with increasing $\Delta T_{\rm eff}$, and exceeds the saturated efficiency $\eta_{\rm sat}$ at a certain temperature, for example, at $T_{\rm eff,h} \approx 895$ K for $\tau_c = 20$ ms. When $\tau_c = 0$, $\eta_a$ is the same as the efficiency of the Stirling engine in a passive bath. As $\tau_c$ increases, the curve of $\eta_a$ also increases and approaches the limiting curve (purple dashed line), indicating that the engine performance is enhanced by the increasing $\tau_c$, as shown in Fig. S7(b). Our measurement (symbols) agrees well with the analytically calculated Eq. (S27) (solid curves). The theoretical validation of the outperformance of the ABHE is provided in Sec. IX of SM [25].

## V. CONCLUSION

An active bath is supposed to have some capability that a passive one does not have. This raises the question of whether the efficiency of a microscopic heat engine could be enhanced when a passive bath is replaced by an active bath. Beyond several recent theoretical studies devoted to this question, this work provides a rare experiment on this problem and shows that the stiffness-dependent noise strength with nonzero correlation could be a crucial factor for the outperformance of an active engine in the quasistatic limit. Our protocol may be implemented using photokinetic bacteria whose activity depends on the light intensity (laser stiffness) [33,34]. The revealed mechanism for high engine efficiency deepens our knowledge

about the impact of an active heat bath. It also suggests insight into understanding the motion of nanomachines and biological motors in complex environments. Furthermore, a recent study shows that engine outperformance could be explained by a Kullback-Leibler distance related term [35]. This term accounts for the entropy production in the hidden degrees of freedom, such as the positions and other variables related to the state of the bacteria in Ref. [15]. It has not been considered as a cost as the normal input heat in the traditional definition of efficiency in most previous studies, including Ref. [15] and the current experiment. Collecting experimental data for the Kullback-Leibler distance and combining their contribution with that of the normal input heat could help understand the origin of the high efficiency found in this study [35].

## ACKNOWLEDGMENTS

This work was supported by the Ministry of Science and Technology, Taiwan, under Grants No. 110-2112-M-008-006-(Y.J.), No. 109-2112-M-008-019-(H.Y.C.), No. 107-2112-M-008-003-MY3(C.H.C.), the National Center for Theoretical Sciences of Taiwan, and individual KIAS Grant No. PG064901 (J.S.L.) at the Korea Institute for Advanced Study.

[1] H. B. Callen, *Thermodynamics and an Introduction to Thermostatistics* (Wiley, New York, 1985).
[2] T. Schmiedl and U. Seifert, Efficiency at maximum power: An analytically solvable model for stochastic heat engines, Europhys. Lett. **81**, 20003 (2008).
[3] V. Blickle and C. Bechinger, Realization of a micrometre-sized stochastic heat engine, Nat. Phys. **8**, 143 (2012).
[4] I. A. Martínez, É. Roldán, Luis Dinis, Dmitri Petrov, J. M. R. Parrondo, and R. A. Rica, Brownian Carnot engine, Nat. Phys. **12**, 67 (2016).
[5] Johannes Roßnagel, S. T. Dawkins, K. N. Tolazzi, O. Abah, E. Lutz, F. Schmidt-Kaler, and K. Singer, A single-atom heat engine, Science **352**, 325 (2016).
[6] J. A. C. Albay, Z.-Y. Zhou, C.-H. Chang, and Y. Jun, Shift a laser beam back and forth to exchange heat and work in thermodynamics, Sci. Rep. **11**, 4394 (2021).
[7] X.-L. Wu and A. Libchaber, Particle Diffusion in a Quasi-Two-Dimensional Bacterial Bath, Phys. Rev. Lett. **84**, 3017 (2000).
[8] G. Ariel, A. Rabani, S. Benisty, J. D. Partridge, R. M. Harshey, and A. Be'er, Swarming bacteria migrate by Lévy walk, Nat. Commun. **6**, 8396 (2015).
[9] K. Kanazawa, T. G. Sano, A. Cairoli, and A. Baule, Loopy Lévy flights enhance tracer diffusion in active suspensions, Nature (London) **579**, 364 (2020).
[10] Y. Sumino, K. H. Nagai, Y. Shitaka, D. Tanaka, K. Yoshikawa, H. Chaté, and K. Oiwa, Large-scale vortex lattice emerging from collectively moving microtubules, Nature (London) **483**, 448 (2012).
[11] T. Sanchez, D. T. N. Chen, S. J. Decamp, M. Heymann, and Z. Dogic, Spontaneous motion in hierarchically assembled active matter, Nature (London) **491**, 431 (2012).
[12] H. Li, Xia-qing Shi, M. Huang, X. Chen, M. Xiao, C. Liu, H. Chaté, and H. P. Zhang, Data-driven quantitative modeling of bacterial active nematics, Proc. Natl. Acad. Sci. USA **116**, 777 (2019).
[13] H.-R. Jiang, N. Yoshinaga, and M. Sano, Active Motion of a Janus Particle by Self-Thermophoresis in a Defocused Laser Beam, Phys. Rev. Lett. **105**, 268302 (2010).
[14] M. Han, J. Yan, S. Granick, and E. Luijten, Effective temperature concept evaluated in an active colloid mixture, Proc. Natl. Acad. Sci. USA **114**, 7513 (2017).
[15] S. Krishnamurthy, S. Ghosh, D. Chatterji, R. Ganapathy, and A. K. Sood, A micrometre-sized heat engine operating between bacterial reservoirs, Nat. Phys. **12**, 1134 (2016).
[16] R. Zakine, A. Solon, T. Gingrich, and F. van Wijland, Stochastic Stirling engine operating in contact with active baths, Entropy **19**, 193 (2017).
[17] V. Holubec, S. Steffenoni, G. Falasco, and K. Kroy, Active Brownian heat engines, Phys. Rev. Res. **2**, 043262 (2020).
[18] G. Gronchi and A. Puglisi, Optimization of an active heat engine, Phys. Rev. E **103**, 052134 (2021).
[19] J. S. Lee and H. Park, Effects of the non-Markovianity and non-Gaussianity of active environmental noises on engine performance, Phys. Rev. E **105**, 024130 (2022).
[20] N. Roy, N. Leroux, A. K. Sood, and R. Ganapathy, Tuning the performance of a micrometer-sized Stirling engine through reservoir engineering, Nat. Commun. **12**, 4927 (2021).
[21] N. Koumakis, C. Maggi, and R. Di Leonardo, Directed transport of active particles over asymmetric energy barriers, Soft Matter **10**, 5695 (2014).
[22] C. Maggi, U. M. B. Marconi, N. Gnan, and R. Di Leonardo, Multidimensional stationary probability distribution for interacting active particles, Sci. Rep. **5**, 10742 (2015).
[23] G. Szamel, Self-propelled particle in an external potential: Existence of an effective temperature, Phys. Rev. E **90**, 012111 (2014).
[24] C. Maggi, M. Paoluzzi, N. Pellicciotta, A. Lepore, L. Angelani, and R. Di Leonardo, Generalized Energy Equipartition in Harmonic Oscillators Driven by Active Baths, Phys. Rev. Lett. **113**, 238303 (2014).
[25] See Supplemental Material at http://link.aps.org/supplemental/10.1103/PhysRevResearch.5.033208 for details about the experimental realization and the calculation of stochastic energetics of passive and active heat engines, which includes Refs. [26,27].
[26] Y. Jun, S. K. Tripathy, B. R. J. Narayanareddy, M. K. Mattson-Hoss, and S. P. Gross, Calibration of optical tweezers for in vivo force measurements: How do different approaches compare? Biophys. J. **107**, 1474 (2014).
[27] K. Sekimoto, Langevin equation and thermodynamics, Prog. Theor. Phys. Suppl. **130**, 17 (1998).
[28] J. S. Lee, J.-M. Park, and H. Park, Brownian heat engine with active reservoirs, Phys. Rev. E **102**, 032116 (2020).
[29] M. Gavrilov, Y. Jun, and J. Bechhoefer, Real-time calibration of a feedback trap, Rev. Sci. Instrum. **85**, 095102 (2014).
[30] J. A. C. Albay, G. Paneru, H. K. Pak, and Y. Jun, Optical tweezers as a mathematically driven spatio-temporal potential generator, Opt. Express **26**, 29906 (2018).

[31] J. R. Gomez-Solano, L. Bellon, A. Petrosyan, and S. Ciliberto, Steady-state fluctuation relations for systems driven by an external random force, Europhys. Lett. **89**, 60003 (2010).

[32] I. A. Martínez, É. Roldán, J. M. R. Parrondo, and D. Petrov, Effective heating to several thousand kelvins of an optically trapped sphere in a liquid, Phys. Rev. E **87**, 032159 (2013).

[33] H. Massana-Cid, C. Maggi, G. Frangipane, and R. Di Leonardo, Rectification and confinement of photokinetic bacteria in an optical feedback loop, Nat. Commun. **13**, 2740 (2022).

[34] Z. Liu, J. Zhang, J. Jin, Z. Geng, Q. Qi, and Q. Liang, Programming bacteria with light-sensors and applications in synthetic biology, Front. Microbiol. **9**, 2692 (2018).

[35] A. Datta, P. Pietzonka, and A. C. Barato, Second Law for Active Heat Engines, Phys. Rev. X **12**, 031034 (2022).